Inorganic Chemistry

Article

pubs.acs.org/IC

Cyanide-Bridged Fe^{III}–Cu^{II} Complexes: Jahn–Teller Isomerism and Its Influence on the Magnetic Properties

Mihail Atanasov,*[,†,‡,§] Peter Comba,*[,†] and Stefan Helmle[†]

[†]Anorganisch-Chemisches Institut, INF 270, Universität Heidelberg, D-69120 Heidelberg, Germany

[‡]Max-Planck-Institut für Chemische Energiekonversion, Stiftstr. 34-36, D-45470 Mülheim an der Ruhr, Germany

[§]Institute of General and Inorganic Chemistry, Bulgarian Academy of Sciences, Acad.Georgi Bontchev Str. Bl.11, 1113 Sofia, Bulgaria

Supporting Information

ABSTRACT: We report here the synthesis and characterization of four dinuclear cyanide-bridged Fe^{III}–Cu^{II} complexes, based on a tetra- or a pentadentate bispidine ligand (L^1 or L^2, respectively; bispidines are 3,7-diazabiyclo[3.3.1]nonane derivatives) coordinated to the Cu^{II} center, and a tridentate bipyridineamide (bpca) coordinated to the *low-spin* Fe^{III} site, with cyanide groups completing the two coordination spheres, one of them bridging between the two metal ions. The four structurally characterized complexes $[\{Fe(bpca)(CN)_3\}\{Cu(L^1{\cdot}H_2O)\}]BF_4$, $[\{Fe(bpca)(CN)_3\}\{Cu(L^2)\}][Fe(bpca)(CN)_3]{\cdot}5H_2O$, $[\{Fe(bpca)(CN)_3\}\{Cu(L^2{\cdot}MeOH)\}]PF_6{\cdot}MeOH{\cdot}H_2O$, and $[\{Fe(bpca)(CN)_3\}\{Cu(L^2)\}]PF_6{\cdot}2H_2O$ belong to different structural isomers. The most important differences are structurally and electronically enforced (direction of the pseudo-Jahn–Teller mode) strong or weak interactions of the copper(II) center with the cyanide bridge. The related strength of the magnetic coupling of the two centers is analyzed with a combination of experimental magnetic, electron paramagnetic resonance (EPR), electronic spectroscopic data together with a ligand-field theory- and density functional theory (DFT)-based analysis.

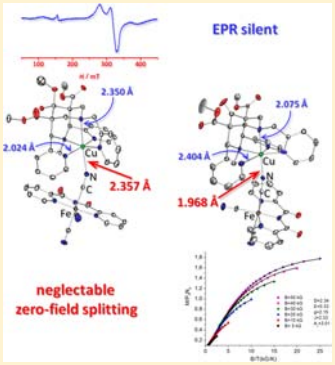

INTRODUCTION

The design, synthesis, and characterization of exchange-coupled oligonuclear complexes is of interest for novel magnetic materials and also to better understand the electronic properties and reactivities of catalysts, specifically also of enzymes and corresponding model systems.[1,2] Cyanide-bridged complexes have the advantage of exclusively forming linear M-CN-M′ subunits and therefore in principle lead to predictable structures, and to a number of structural motifs with interesting electronic and magnetic properties.[3,4] The theory of magnetic exchange mechanisms across the cyanide bridge has been studied in detail,[5] and we recently have reported a rare set of cyanide-bridged dicopper(II) complexes, which allowed us to fully characterize the electronic properties as a function of the coordination geometry of the metal centers and their relative orientation.[6] From the detailed experimental and ligand-field based analysis it was also possible to quantitatively determine and fully understand the zero-field splitting, and this is of some importance in the context of the classical analysis of copper acetate and a recent redetermination of the sign of the zero-field splitting by high-field EPR,[7,8] and, of course, also is of great interest in the field of single-molecular magnetism.[9,10]

The above-mentioned cyanide-bridged dicopper(II) complexes were based on bispidine complexes (see Chart 1 for the chemical structure of the bispidine ligands [3,7-diazabiyclo[3.3.1]nonane derivatives] used in this Article). These have been studied in detail in recent years, specifically also in terms of the unique reactivities, complex stabilities and selectivities, and structural properties of the corresponding transition metal complexes.[11] A unique feature of the copper(II) complexes is that there are three distinct and, dependent on the specific bispidine ligand used, close to degenerate isomers in terms of the electronically enforced elongation of a specific copper-donor axis.[12,13] As a result, it is in principle possible to tune the Cu-NC distance and Cu-NC-M′ orientation in heterodinuclear complexes, and this is the basis of the work reported here. In the series of four Cu^{II}-NC-

Chart 1. Structure and Numbering of the Ligands

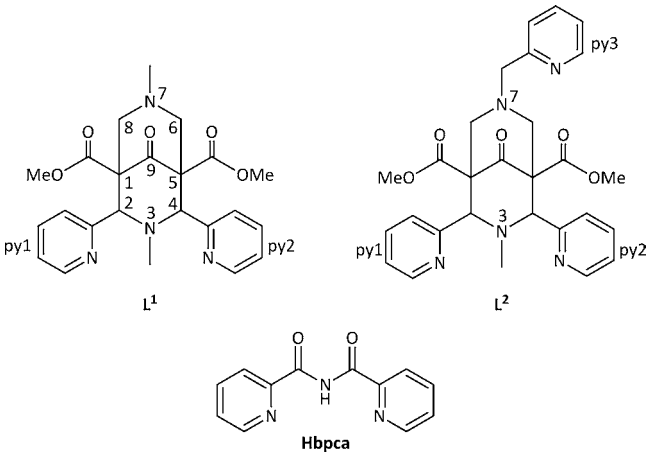

Received: May 29, 2012
Published: August 20, 2012

   dx.doi.org/10.1021/ic301122h | *Inorg. Chem.* 2012, 51, 9357–9368

Fe^{III} structures, where Cu^{II} is coordinated to a tetra- or pentadentate bispidine and the Fe^{III} center is coordinated to bipyridineamide (bpca, see Chart 1) and two additional cyanide groups, the Cu^{II}-NC distance varies from 1.93 to 2.38 Å, that of Fe^{III}−CN from 1.92 Å to 1.97 Å, and the corresponding Cu−N−C angles differ between the extremes of 173° and 155°.

As expected (see discussion of the structural properties below), the various possible isomers are very similar in energy. Therefore, it was difficult to prepare and study (structures, magnetism, electronic, infrared and electron paramagnetic resonance (EPR) spectroscopies) a set of isomers with otherwise identical composition. For example, it is known that, depending on the solvent used and also dependent on the coordinated metal ion, the ketone at C9 may be hydrolyzed or in methanol, often a hemiacetal is observed.[11,14,15] Also, this is known to have a significant influence on the donor properties of the tertiary amine groups and therefore may significantly change the electronic properties.[11,16,17] We report here the full experimental characterization of a set of four heterodinuclear complexes with similar but not identical composition. For the theoretical analysis, we refer to earlier work with analogous systems[11,18] and base our interpretation on a density functional theory (DFT)- and ligand-field-based analysis.

RESULTS AND DISCUSSION

Syntheses and Structural Properties. The reaction of $[N(^tbu)_4][Fe^{III}(bpca)(CN)_3]$ with $[Cu(L^1)(NCMe)(OH_2)](PF_6)_2$ in a mixture of MeCN and CH_2Cl_2, or with $[Cu(L^1)(OH_2)_2](BF_4)_2{\cdot}H_2O$ in MeOH, produced the heterodinuclear complexes $[\{Fe(bpca)(CN)_3\}\{Cu(L^1)\}]PF_6{\cdot}2H_2O$ and $[\{Fe(bpca)(CN)_3\}\{Cu(L^1{\cdot}H_2O)\}]BF_4$, respectively.[19] This species has the cyanide bridge *trans* to N3 of the bispidine-copper(II) complex, the bridging cyanide in *cis* position to the other 2 cyanides of the iron(III) subunit, and the Jahn−Teller-elongated axis of the copper(II) chromophore along Cu−N7 (see panel (a) in Figure 1, throughout we use the nomenclature *N3-cis-N7* isomer for this structure). With the pentadentate bispidine ligand L^2, three different structural isomers of the dinuclear complex were isolated: (i) In MeCN/CH_2Cl_2 (1:0.8) with slow crystallization at room temperature the *N7-cis-N7* isomer is produced (cyanide bridge *trans* to N7, bridging cyanide *cis* to the other two cyanides of the iron(III) core, Jahn−Teller axis along Cu−N7, see panel (b) in Figure 1). (ii) With MeOH as solvent and ether diffusion at room temperature, the *N7-trans-N7* isomer was obtained (see panel (c) in Figure 1; note that at C9 of the bispidine, this is a methanolated ligand). (iii) With MeCN/CH_2Cl_2 (1:2) and ether diffusion at 4 °C the *N7-trans-py* isomer results (see panel (c) in Figure 1, Jahn−Teller axis of the copper(II) site along py1-Cu-py2). Because the various isomers are very similar in energy (see Introduction), it is not unexpected that the isolation of single crystals of the three isomers is not fully reproducible.[20] ORTEP plots of all experimentally determined structures appear in Figure 1, and selected structural data are listed in Table 1.

N3-cis-N7 Isomer: [{Fe(bpca)(CN)$_3$}{Cu(L^1·H$_2$O)}]BF$_4$. The precursor $[Cu(L^1)(OH_2)_2]^{2+}$ provides two possible coordination sites for a CN^--bridge to $[Fe^{III}(bpca)(CN)_3]^-$, that is, *trans* to N7 or *trans* to N3. As expected, in $[\{Fe(bpca)(CN)_3\}\{Cu(L^1{\cdot}H_2O)\}]BF_4$ the formation of the CN-bridge occurs perpendicular to the Jahn−Teller axis of the Cu^{II}-site, and the most stable Jahn−Teller isomer has the elongation along Cu−N7 and therefore the coligand *trans* to N3 with a short and strong Cu-NC bond.[6,12,13,21,22] This leads to a relatively short Cu···Fe distance of 4.995 Å and a nearly linear bridge (Cu−N−C 173.0° and Fe−C−N 177.9°). There is an additional very weak interaction of the Cu^{II} center to an axial fluoride of the BF_4^- ion (2.980 Å).

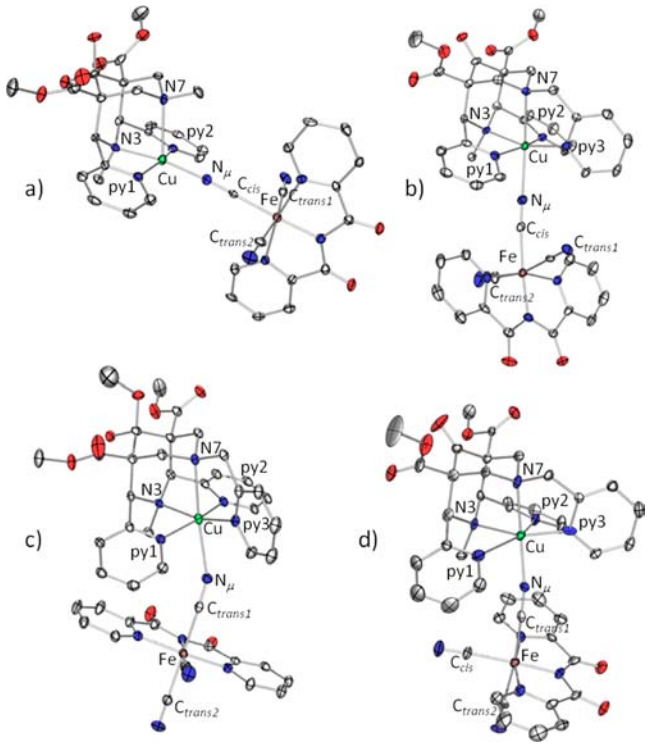

Figure 1. Pov-ray plots[63] of the dinuclear units of (a) $[\{Fe(bpca)(CN)_3\}\{Cu(L^1{\cdot}H_2O)\}]^+$ (*N3-cis-N7*), (b) $[\{Fe(bpca)(CN)_3\}\{Cu(L^2)\}][Fe(bpca)(CN)_3]$ (*N7-cis-N7*), (c) $[\{Fe(bpca)(CN)_3\}\{Cu(L^2{\cdot}MeOH)\}]PF_6$ (*N7-trans-N7*), (d) $[\{Fe(bpca)(CN)_3\}\{Cu(L^2)\}]PF_6$ (*N7-trans-py*); thermal ellipsoids at 30% probability, H atoms omitted.

N7-cis-N7 Isomer: [{Fe(bpca)(CN)$_3$}{Cu(L^2)}][Fe(bpca)(CN)$_3$]·5H$_2$O. With the pentadentate bispidine L^2 and the often observed Jahn−Teller elongation along Cu−N7,[13,22] the bridging cyanide is "on the Jahn-Teller axis" (Cu-NC = 2.302 Å vs 1.931 Å in the *N3-cis-N7* and 1.964 Å in the *N7-trans-py* isomers). This leads to a comparatively long Cu···Fe distance of 5.215 Å and a significantly bent cyanide bridge (Cu−N−C = 154.7°, Fe−C−N = 174.5°).

N7-trans-N7 Isomer: [{Fe(bpca)(CN)$_3$}{Cu(L^2·MeOH)}]PF$_6$·MeOH·H$_2$O. Here, one of the *transoid* cyanides of the iron(III) core bridges to the copper(II) center. The Cu^{II} chromophore is very similar to that of the *N7-cis-N7* isomer. However, there are significant but small differences of the geometry around Fe^{III}, and this is primarily due to the Fe-CN distance of the bridging cyanide and leads to a somewhat longer Cu···Fe distance (5.350 Å vs 5.215 Å).

N7-trans-py Isomer: [{Fe(bpca)(CN)$_3$}{Cu(L^2)}]PF$_6$·2H$_2$O. Here, the copper(II) chromophore is different from the other three structures; in terms of the cyanide bridge, it has, as expected, similarities with the L^1-based *N3-cis-N7* isomer, that is, a short Cu-NC distance (1.968 Å vs 1.931 Å vs >2.0 Å). Therefore, the bridge is also more linear than for the *N7-cis/trans-N7* isomers and similar to the *N3-cis-N7* isomer (Cu−N−C = 169° vs 173° vs 154°). It is known that, induced by the strong ligand field of cyanide, a switch of the Jahn−Teller-

dx.doi.org/10.1021/ic301122h | Inorg. Chem. 2012, 51, 9357−9368

Table 1. Selected Structural Parameters of $[\{Fe(bpca)(CN)_3\}\{Cu(L^1{\cdot}H_2O)\}]BF_4$ (*N3-cis-N7* isomer), $[\{Fe(bpca)(CN)_3\}\{Cu(L^2)\}][Fe(bpca)(CN)_3]$ (*N7-cis-N7* isomer), $[\{Fe(bpca)(CN)_3\}\{Cu(L^2{\cdot}MeOH)\}]PF_6$ (*N7-trans-N7* isomer), and $[\{Fe(bpca)(CN)_3\}\{Cu(L^2)\}]PF_6$ (*N7-trans-py* isomer)[a]

	$[\{Fe(bpca)(CN)_3\}\{Cu(L^1{\cdot}H_2O)\}]BF_4$	$[\{Fe(bpca)(CN)_3\}\{Cu(L^2)\}][Fe(bpca)(CN)_3]$	$[\{Fe(bpca)(CN)_3\}\{Cu(L^2{\cdot}MeOH)\}]PF_6$	$[\{Fe(bpca)(CN)_3\}\{Cu(L^2)\}]PF_6$
	N3-cis-N7	*N7-cis-N7*	*N7-trans-N7*	*N7-trans-py*
		Distances [Å]		
Cu–N(3)	2.009(5)	2.050(3)	2.049(2)	2.131(6)
Cu–N(7)	**2.301(5)**	**2.381(4)**	**2.350(2)**	2.075(8)
$Cu–N_{py1}$	1.956(5)	2.003(4)	2.029(2)	**2.329(7)**
$Cu–N_{py2}$	1.964(5)	2.056(4)	2.024(3)	**2.404(7)**
$Cu–N_{py3}$	**(2.981)**[b]	2.024(4)	2.043(3)	1.965(7)
$Cu–N_{\mu}$	1.932(6)	**2.301(5)**	**2.375(3)**	1.968(8)
C–N	1.161(7)	1.134(6)	1.153(4)	1.181(10)
Cu···Fe	4.995(2)	5.216(1)	5.350(1)	5.071(2)
$Fe–C_{cis}$	1.915(7)	1.924(6)	1.956(4)	1.945(8)
$Fe–C_{trans1}$	1.940(8)	1.972(6)	1.968(3)	1.961(11)
$Fe–C_{trans2}$	1.930(8)	1.978(6)	1.946(3)	1.933(11)
$Fe–N_{Amid}$	1.856(5)	1.872(4)	1.902(3)	1.872(6)
$Fe–N_{py4}$	1.967(5)	1.981(4)	1.969(2)	1.953(7)
$Fe–N_{py5}$	1.977(5)	1.973(4)	1.961(2)	1.952(7)
		Angles [deg]		
Cu–N–C	173.2(4)	154.6(4)	154.5(2)	168.9(7)
Fe–C–N	177.9(5)	174.5(4)	176.4(3)	173.5(7)

[a]Standard deviations in brackets, the Jahn-Teller-elongated bonds of the Cu^{II} centers are bold. [b]Weak bond to a fluoride of BF_4^-.

dx.doi.org/10.1021/ic301122h | *Inorg. Chem.* 2012, 51, 9357–9368

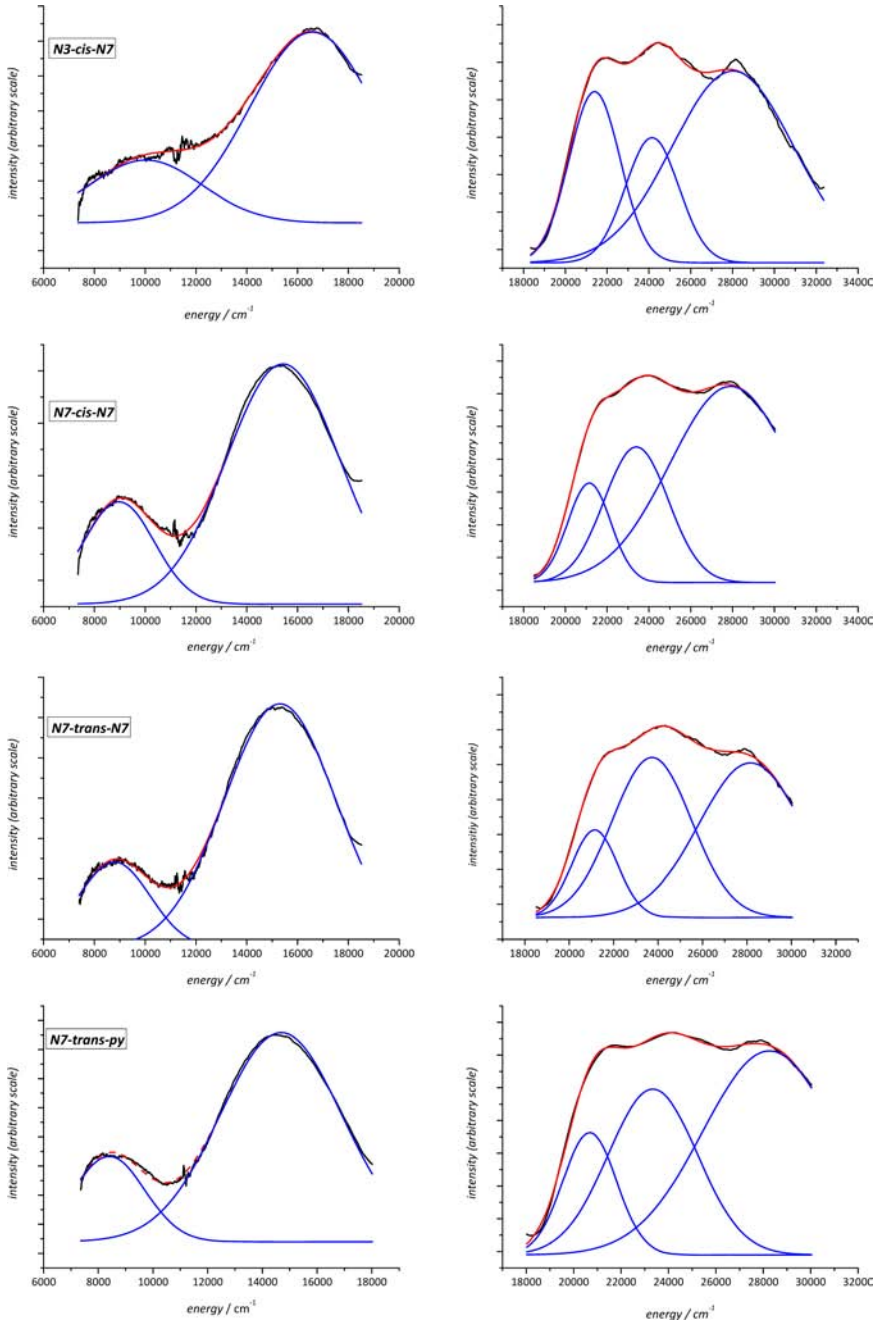

Figure 2. Gaussian analysis of the copper(II) (left) and iron(III) areas (right) of the electronic spectra of $[\{Fe(bpca)(CN)_3\}\{Cu(L^1{\cdot}H_2O)\}]^+$ (*N3-cis-N7*), $[\{Fe(bpca)(CN)_3\}\{Cu(L^2)\}][Fe(bpca)(CN)_3]$ (*N7-cis-N7*), $[\{Fe(bpca)(CN)_3\}\{Cu(L^2{\cdot}MeOH)\}]PF_6$ (*N7-trans-N7*), and $[\{Fe(bpca)(CN)_3\}\{Cu(L^2)\}]PF_6$ (*N7-trans-py*); experimental (solid state): black, Gaussian fit: red; simulated transitions: blue; see Table 2 for the fitted energies and Supporting Information for details of the Gaussian analysis and the full experimental spectra.

elongated axis from N7−Cu to py1-Cu-py2 can occur.[6,18] The important result here is that the Cu···Fe distances (and concomitantly the Cu-NC distance and the Cu−N−C angle) differ considerably with 5.350 Å vs 5.071 Å (*N7-trans-py* vs *N7-trans-N7* isomer).

Single-point DFT calculations were used to compute electronic parameters (see below), and the energies of these (see Supporting Information) may be used as an indication of the relative stabilities.[23,24] It appears that the *N7-trans-N7* and the *N7-cis-N7* isomers are truly degenerate, and this is not unexpected, but the *N7-trans-py* isomer is significantly less stable (by about 30 kJ/mol with an assumed error limit of around 20−25 kJ/mol). The fact that the three structures are very similar in energy indicates that it must be difficult to develop a strategy for selective isolation of one of the isomers; moreover, it is difficult to reliably and reproducibly prepare a sample of the least stable (and most interesting) *N7-trans-py* isomer.[20]

In conclusion, the four isomers (three with the pentadentate L^2-based system) lead to remarkable structural differences, which are expected to lead to striking differences with respect to the electronic ground and excited states and magnetic exchange. The orientation of the bridging cyanide related to the Jahn−Teller elongated axis leads to large differences in the Cu−

dx.doi.org/10.1021/ic301122h | *Inorg. Chem.* 2012, 51, 9357−9368

N−C−Fe axis (Cu−N, Fe−C and Cu···Fe distances, Cu−N−C and Fe−C−N angles): there are short distances when the bridging cyanide is perpendicular to the Jahn−Teller axis (*N3-cis-N7 and N7-trans-py* isomers: Cu···Fe = 5.0 and 5.1 Å vs 5.2 and 5.4 Å) and concomitantly, the Cu···Fe axis is quite linear (Cu−N−C = 173 and 169° vs 155°). The influence of these structural features on the electronics is now described.[25−27]

Spectroscopy and Magnetism. The infrared spectra of the four dinuclear complexes have the expected characteristic CN stretching bands of bridging and terminal cyanide ligands (see Supporting Information for the spectra).[28] For [{Fe(bpca)$(CN)_3$}{Cu(L^1)}]PF_6·$2H_2O$ (*N3-cis-N7* isomer) there are three CN signals, two bands appear at 2120 cm^{-1} and 2126 cm^{-1}, assigned to the terminal cyanide ligands (our measurement of the precursor [N(^{t}bu)$_4$][Fe^{III}(bpca)$(CN)_3$] shows two bands at 2123 cm^{-1} and 2138 cm^{-1},[29] and one at 2122 cm^{-1}). One transition is shifted to higher energy (2173 cm^{-1}) and is therefore assigned to the bridging cyanide. The *N7-trans-py* isomer of the L^2-based system also features three cyanide vibration modes with two bands at 2129 cm^{-1} and 2117 cm^{-1}, assigned to the terminal cyanide groups. The third band appears at slightly higher energy (2144 cm^{-1}) and is believed to be due to the bridging cyanide ligand. Compared to the L^1 based *N3-cis-N7* system, this is 29 cm^{-1} lower in energy, and this may be related to a significantly longer Cu-NC bond (1.97 vs 1.93 Å vs >2.3 Å for the other isomers). Consistent with this observation a shift of the stretching mode for the bridging cyanide could not be observed for the other two isomers (*N7-cis-N7* and *N7-trans-N7*). These both show IR spectra similar to that one of the precursor (2120 cm^{-1}, 2126 cm^{-1}),[29] with two bands at 2127 cm^{-1}, 2135 cm^{-1} (*N7-trans-N7*) and 2124 cm^{-1}, 2133 cm^{-1} (*N7-cis-N7*). For the *cis*-isomer an additional shoulder at 2143 cm^{-1} probably is due to a small impurity of the *N7-trans-py* isomer (similar synthetic procedure).

The electronic spectra of the four Cu^{II}-Fe^{III} species (powder spectra, see Figure 2 and Supporting Information) exhibit the expected electronic transitions for the *low-spin* Fe^{III} and Cu^{II} subunits; the corresponding energies from a simulation by three and two Gaussian envelopes (see Figure 2), respectively, are listed in Table 2. Two d-d transitions of the Cu^{II} centers are clearly visible for all four complexes. In a local *pseudo-D_{4h}* symmetry they are assigned to the $^2B_{1g} \leftarrow {}^2A_{1g}$ transition observed at energies between approximately 8,400 and 9,000 cm^{-1} for the L^2-based six-coordinate and 10,000 cm^{-1} for the L^1-based system (see Figure 2). The second band at higher energies belongs to the $^2B_{1g} \leftarrow {}^2E_g, {}^2B_{2g}$ transition, between approximately 14,700 cm^{-1} for the *N7-trans-py* isomer (L^2-based system) and 16,600 cm^{-1} for the *N3-cis-N7* isomer (L^1-based system). As anticipated, for the *N7-trans-N7* and the *N7-cis-N7* isomers the energies of both transitions are very similar with 8,800 cm^{-1} and 15,300 cm^{-1} for the former, and 9,000 cm^{-1} and 15,400 cm^{-1} for the latter (see Figure 2). However, for the two "Jahn-Teller isomers" (*N7-trans-N7* and *N7-trans-py*) there are remarkably large differences in both transition energies, with the latter being shifted to lower energy with respect to the former by 400 cm^{-1} ($^2B_{1g} \leftarrow {}^2A_{1g}$) and 600 cm^{-1} ($^2B_{1g} \leftarrow {}^2E_g, {}^2B_{2g}$, see Figure 2). Since the py1-Cu-py2 axis is elongated in the *N7-trans-py* isomer, there is a weakening of the π-back-donation of the pyridine donors which leads to a smaller splitting of the t_{2g}- and e_g-orbitals (in O_h-symmetry). Between 20,000 and 30,000 cm^{-1} all four spectra are dominated by electronic transitions due to Fe^{III}, with at least three maxima of strongly overlapping bands (see Figure 2 and Table 2). These are assigned to electronic transitions from the $^2T_{2g}$ ground state of *low-spin* Fe^{III} (octahedral notations) to at least 9 excited states originating from the $^2A_{2g}$, $^2T_{1g}$, ^2E_g, and $^2T_{2g}$ octahedral parent terms (see Supporting Information).[30]

The two species with strongly coupled metal centers (*N3-cis-N7* (L^1) and *N7-trans-py* (L^2)) are EPR silent, and this was expected because of a relatively large zero-field splitting of a few wavenumbers, emerging from the SQUID measurements (see below). With the two compounds with the cyanide bridge "on the Jahn-Teller axis", *N7-cis-N7* and *N7-trans-N7* EPR spectra are observed but only the latter has a quality (line width) which allowed a thorough analysis (Figure 3). This is based on spectra

Table 2. Energies of Cu^{II} and *low-spin* Fe^{III} Based d-d Transitions from a Simulation of Ambient Temperature Diffuse Reflectance Spectra by Two and Three Gaussian Envelopes

isomer	*N3-cis-N7*	*N7-cis-N7*	*N7-trans-N7*	*N7-trans-py*
Cu^{II}	10,000	9,000	8,800	8,400
	16,600	15,400	15,300	14,700
Fe^{III}	21,400	21,150	21,150	20,700
	24,150	23,400	23,700	23,350
	28,000	27,900	28,150	28,250

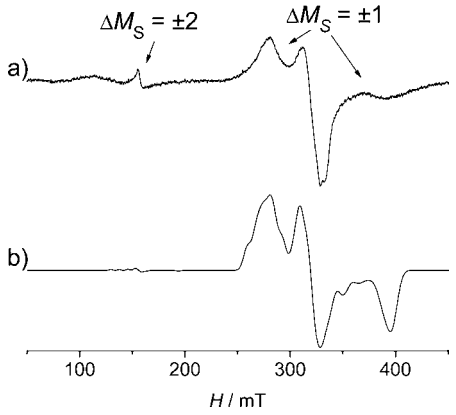

Figure 3. EPR spectra of [{Fe(bpca)$(CN)_3$}{Cu(L^2·MeOH)}]PF_6 (*N7-trans-N7* isomer); (a) experimental (undiluted solid, 6 K, ν = 9.414239 GHz; (b) simulated (parameters see Table 2; spin Hamiltonian, see eq 2, 3; details, see Experimental Section).

simulation (see Experimental Section for details),[31] based on the spin Hamiltonian of eqs 1−3.

$$\hat{H}_{\text{Total}} = \sum_{i=1}^{2} \hat{H}_i + \hat{H}_{\text{Int}} \quad (1)$$

$$\hat{H}_i = \mu_B \mathbf{B}\cdot\mathbf{g_i}\cdot\mathbf{S_i} \quad (2)$$

$$\hat{H}_{\text{Int}} = -J\mathbf{S}_1\cdot\mathbf{S}_2 + \mathbf{S}_1\cdot\mathbf{J}_{12}\cdot\mathbf{S}_2 + \mathbf{A}_{12}\cdot\mathbf{S}_1 \times \mathbf{S}_2 \quad (3)$$

Because of the small ferromagnetic coupling (J = 1.8 cm^{-1}, see Table 2), at 6 K there is only a weak signal around 250−400 mT of the triplet ground state, which decreases and eventually disappears when the excited state is populated with increasing temperature. In addition, at around 150 mT (half-field) there is a weak transition due to $\Delta M_S = \pm 2$. Because of the weakness of the coupling, it was not necessary to consider anisotropic exchange (J_{12}) in the simulation, and the very small zero-field

dx.doi.org/10.1021/ic301122h | *Inorg. Chem.* 2012, 51, 9357−9368

splitting was simulated with pure dipole−dipole coupling (D_{dip}). However, because of the strongly distorted geometry, it was necessary to consider antisymmetric exchange (A_{12}). The parameters obtained from EPR spectroscopy (Table 3) are in good agreement with those from the magnetic measurements discussed now and are also reasonably well reproduced by the ligand field calculations.

Table 3. Experimentally Determined and Calculated (Parentheses) EPR Parameters of $[\{Fe(bpca)(CN)_3\}\{Cu(L^2{\cdot}MeOH)\}]PF_6$ (*N7-trans-N7* Isomer)

	g_x	g_y	g_z
Cu	2.062(2.038)	2.065(2.056)	2.230(2.287)
Fe	1.42(1.780)	2.29(2.24)	2.50(2.55)
J^a	1.80		
$D_{dip}{}^a$	−0.023[b]		
$A_x{}^a$	0.19		
$A_y{}^a$	0.24		
$A_z{}^a$	0.35		

[a]In cm^{-1}. [b]Based on the experimentally known Fe···Cu distance (5.350 Å).

Measurements of the magnetic susceptibility were done on powdered crystals at 500 G and in the temperature range of 2−300 K. There are two strikingly different sets of $\chi_M T$ vs T curves, those of the *N7-trans-N7 and the N7-cis-N7* isomers with long Cu-NC bonds (Figure 4a and b), and those of the *N3-cis-N7* and the *N7-trans-py* isomers with short Cu-NC bonds (Figure 4c and d; the parameters used to simulate the data with the Bleaney−Bowers approach[7] are given in Table 4). For the two isomers in Figure 4, with relatively long Cu···Fe axes, upon cooling, the $\chi_M T$ values decrease to a minimum at around 30 K (typical contribution of a temperature independent paramagnetism, χ_{TIP}), and then increase again on further cooling to 2 K, as expected for a weak ferromagnetic coupling between the two metal centers.[32] The room temperature $\chi_M T$ value of the *N7-trans-N7* isomer ($\chi_M T$ (300 K) = 1.0 cm^3 K mol^{-1}) is in the expected range for two uncoupled $S = 1/2$ centers (spin-only value: 0.75 cm^3 K mol^{-1}), with a g-value slightly larger than the g-factor of the free electron. For the *N7-cis-N7* isomer the room temperature $\chi_M T$ value of 1.468 cm^3 K mol^{-1} is consistent with three $S = 1/2$ centers (two *low-spin* Fe^{III} and one Cu^{II}). Using the Bleaney−Bowers approach,[7] with the isotropic exchange spin Hamiltonian $H = -J\,\boldsymbol{S}_1{\cdot}\boldsymbol{S}_2$ ($S_1 = S_2 = 1/2$), the magnetic susceptibility data are reproduced with reasonable accuracy (see Figure 4 and Supporting Information). The values of J are positive, except for *N7-trans-py* (see below), that is the coupling through Cu-NC-Fe is ferromagnetic, and this is expected because of the orthogonality between the σ-type Cu^{II} and the π-type Fe^{III} magnetic orbitals. The value of J for *N3-cis-N7* (J = 14.2 cm^{-1}) compares well with published data of Cu^{II}−*low-spin* Fe^{III} exchange coupled systems with similar Cu-NC-Fe bridging topology but variable nuclearities (Table 5). It has been attempted to correlate these changes of J

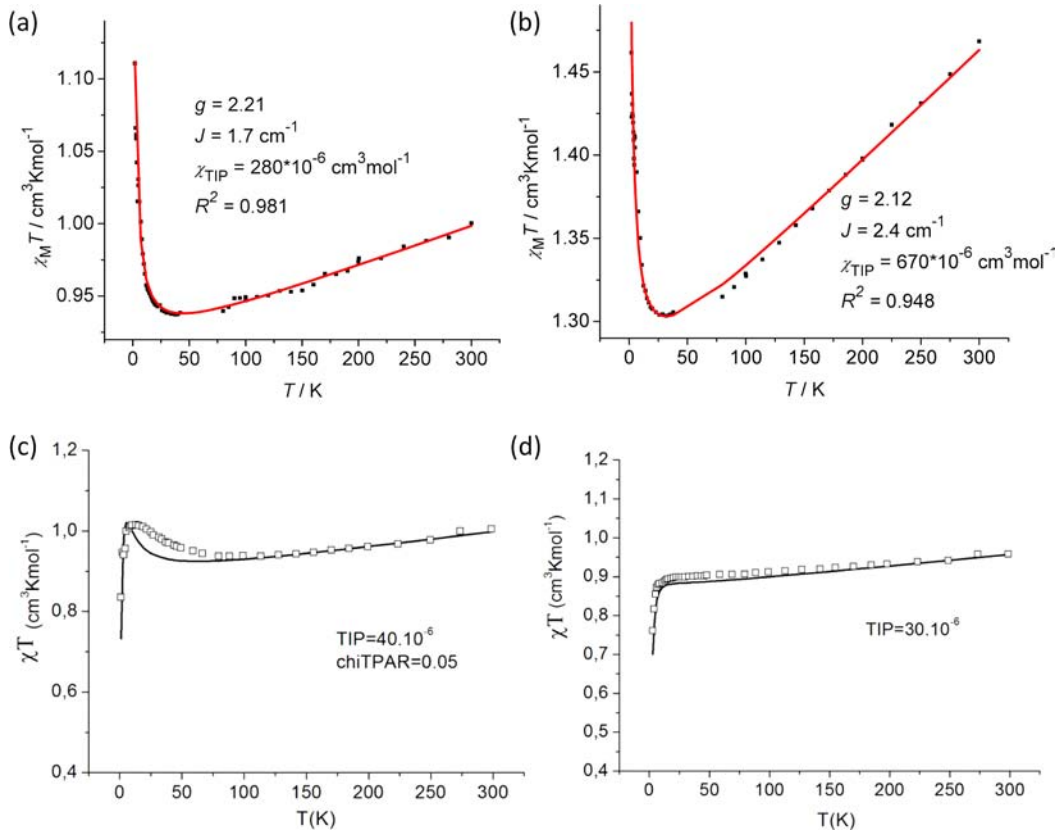

Figure 4. Magnetic susceptibility as a function of temperature ($\chi_M T$ vs T plots) of (a) $[\{Fe(bpca)(CN)_3\}\{Cu(L^2{\cdot}MeOH)\}]PF_6$ (*N7-trans-N7* isomer), (b) $[\{Fe(bpca)(CN)_3\}\{Cu(L^2)\}][Fe(bpca)(CN)_3]$ (*N7-cis-N7* isomer), (c) $[\{Fe(bpca)(CN)_3\}\{Cu(L^1)\}]PF_6$ (*N3-cis-N7* isomer), (d) $[\{Fe(bpca)(CN)_3\}\{Cu(L^2)\}]PF_6$ (*N7-trans-Npy* isomer); the calculated curves of (a), (b) are Bleaney−Bowers fits, and (c), (d) are calculated using the anisotropic parameters from Table 4 with additional TIP and paramagnetic corrections (see text for details).

dx.doi.org/10.1021/ic301122h | Inorg. Chem. 2012, 51, 9357−9368

Table 4. Experimentally Determined and Computed Electronic Parameters of the Four L^1 and L^2 Based Heterodinuclear Complexes

	$[\{Fe(bpca)(CN)_3\}\{Cu(L^1)\}]PF_6$	$[\{Fe(bpca)(CN)_3\}\{Cu(L^2)\}][Fe(bpca)(CN)_3]$	$[\{Fe(bpca)(CN)_3\}\{Cu(L^2{\cdot}MeOH)\}]PF_6$	$[\{Fe(bpca)(CN)_3\}\{Cu(L^2)\}]PF_6$
	N3-cis-N7	*N7-cis-N7*	*N7-trans-N7*	*N7-trans-py*
g_{iso}	2.13[a]/2.09[b]	2.12[a]	2.21[a]/2.09[c]	2.19[a]/2.15[b]
J_{exp} [cm^{-1}]	14.2[a]/3.08[b]	2.4[a]	1.7[a]/1.8[c]	−0.5[a]/2.33[b]
J_{DFT} [cm^{-1}]	14	2	2	−10
D [cm^{-1}]	−4.49[b]		−0.023[c]	2.34[b]
E [cm^{-1}]	−0.41[b]			0.33[b]
A_y [cm^{-1}]	−0.50			3.01

[a]Derived from the magnetic susceptibilities (based on a Bleaney−Bowers approach, for the data and fits, see Supporting Information). [b]Derived from the reduced magnetization with an anisotropic model (see text and Figure 5). [c]Obtained by the simulation of the EPR spectra; g_{iso} is the average of the g values from the EPR simulation, see Table 2.

Table 5. Spin Ground States (S), Cu-NC-Fe Exchange Coupling Parameters J (cm^{-1}), and the Cu−N−C Angles in Cu^{II}−*low-spin* Fe^{III} Exchange Coupled Complexes of Variable Nuclearity

complex	Cu_2Fe (*trans*)	Cu_3Fe_2	Cu_3Fe_2	CuFe *N3-cis-N7*	Cu_2Fe (*cis*)	Cu_2Fe_2	Cu_2Fe_2	Cu_3Fe_2	Cu_2Fe_2
S	3/2	5/2	5/2	1	3/2	2	2	5/2	2
J	18.8	17.0	15.8	14.2	14.1	12.6	9.8	6.9	5.0
∠Cu−N−C[a]	168.4	168.1	167.6	173.2	162.4	171.9	172.3	168.0	164.6
	173.6	178.6	178.8		167.6	176.3	173.5	177.1	
reference	18	59	60	this work	18	61	62	60	32

[a]The lowest and largest values are listed when multiple values exist.

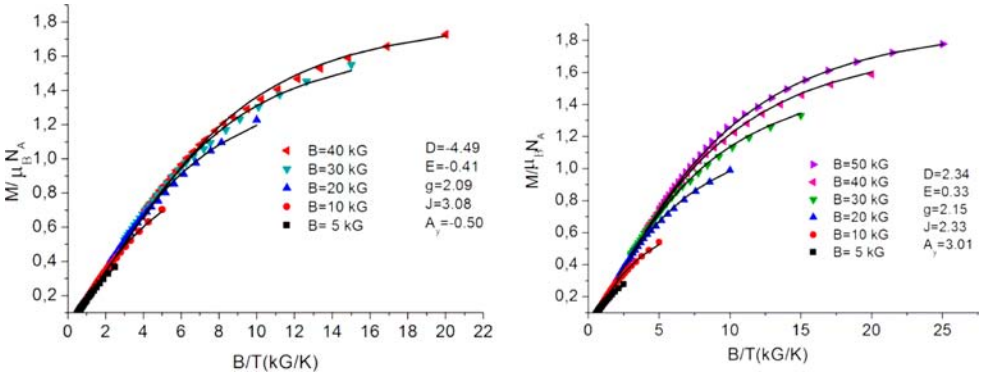

Figure 5. Experimental (symbols, see caption for the applied field) and fitted (black lines) data of the magnetization as a function of B/T; left: $[\{Fe(bpca)(CN)_3\}\{Cu(L^1)\}]PF_6$ (*N3-cis-N7* isomer) and right: $[\{Fe(bpca)(CN)_3\}\{Cu(L^2)\}]PF_6$ (*N7-trans-py* isomer).

with the Cu−N−C angle which varies over a larger range than the correspondig Fe−C−N angle (increasing deviations from linearity is correlated with decreasing J). From the available data it follows that these are not correlated (Table 5 and Supporting Information). Measurements of the reduced magnetization of the two isomers with longer Cu···Fe distances, *N7-cis-N7* and *N7-trans-N7* did not show any splitting of the iso-field lines, that is, the zero-field splitting is, due to the weak coupling, neglectably small (see Supporting Information).

The two more strongly coupled systems (*N3-cis-N7* and *N7-trans-py* isomers) show a significant splitting of the iso-field lines in the measurement of reduced magnetization (see Figure 5), and this allowed us to determine the zero-field splitting parameters (see Table 4). Use was made of the spin-Hamiltonian $\mathbf{H}_S$ of eq 4,

$$\mathbf{H}_S = \begin{array}{c} \begin{matrix} |1,-1\rangle & |1,0\rangle & |1,-1\rangle & |0,0\rangle \end{matrix} \\ \begin{bmatrix} -J/4+D-g\mu_B H_z & (H_x+iH_y)/\sqrt{2} & E & A_y \\ (H_x-iH_y)/\sqrt{2} & -J/4 & (H_x+iH_y)/\sqrt{2} & 0 \\ E & (H_x-iH_y)/\sqrt{2} & -J/4+D+g\mu_B H_z & A_y \\ A_y & 0 & A_y & 3J/4 \end{bmatrix} \end{array} \quad (4)$$

where, in addition to the usual isotropic Zeeman term, the anisotropic zero-field splitting Hamiltonian with axial D and orthorhombic E and an antisymmetric exchange term A_y are taken into account (A_z and A_x are zero by symmetry, see below).[33] It has been shown that A_y terms can become exceedingly large in dinuclear Cu-NC-Fe units, where large distortions at the Fe^{III} site, as they are observed here, impose a lower symmetry of the entire Cu-NC-Fe system.[34] In agreement with this expectation but in contrast to the *N3-cis-N7* isomer, the magnetic data of the *N7-trans-py* complex could not be reproduced, when the A_y term was neglected. Using the Hamiltonian of eq 4, we see acceptable fits of the isothermal magnetization data for both *N3-cis-N7* and *N7-trans-py* emerge

dx.doi.org/10.1021/ic301122h | Inorg. Chem. 2012, 51, 9357−9368

(see Figure 5, parameters listed in Table 4): A negative D value for *N3-cis-N7* but a positive D emerge for *N7-trans-py*, with a significant orthorhombic parameter E in both cases. The most striking difference between the *N3-cis-N7* and *N7-trans-py* isomeric forms is the large anisotropic exchange parameter A_y in the *N7-trans-py* complex (see Table 4). The parameter sets deduced from the magnetization data reproduce the magnetic susceptibility curves of the *N3-cis-N7* and *N7-trans-py* isomers acceptably well (Figure 4). Because of the large A_y and the positive D values of *N7-trans-py*, the increase of χT with decreasing temperature, predicted and observed for the *N3-cis-N7* isomer (D < 0, small value of A_y), becomes largely suppressed. Because of the large zero-field splitting we can conclude that a Bleaney–Bowers fit is not appropriate for the *N3-cis-N7* and *N7-trans-py* isomers with strongly coupled Cu^{II}-Fe^{III} pairs. We have also computed the exchange coupling constant J with the well-established and validated broken symmetry DFT approach.[35] However, the accuracy of these calculations does not allow to fully validate experimentally determined exchange coupling constants in a range of only 15 cm^{-1}.

Ligand Field Analysis. *Cu^{II} Sites.* The angular overlap model (AOM) with a $1/R^6$ dependence of the AOM parameters e_σ and e_π on metal–ligand distance (R)[36] has been used to extract information about the Cu-ligand bond from the energies of the two d-d transitions (see Figure 2 and Table 2). The results show an overall decrease of the σ and π donor strengths across the series of six-coordinate Cu^{II} complexes (isomers *N7-cis-N7*, *N7-trans-N7*, and *N7-trans-py*), with e_σ parameters in the range of values reported for similar Cu^{II} complexes (e_σ = 3,800–5,400 cm^{-1}) but with distinctly larger e_π values than in other systems.[6,36–39] With the parameters from Table 6, ligand field matrices have been calculated based on the geometries from the X-ray analyses (see ref 6 for computational details). In combination with spin–orbit coupling, g-tensor values and their orientation were deduced from these matrices (see Supporting Information). There is good agreement between the calculated and the simulated Cu^{II} g-tensor values of the *N7-trans-N7* isomer (see Table 3).

Table 6. AOM Parameters for Cu^{II} (Deduced from a Fit to the Two Electronic Transitions), and Unique Set of AOM Parameters Used in the Simulation of the d-d Spectra and the Magnetic g-Tensors of the Fe^{III} Site of the Cu–Fe Dinuclear Complexes[a]

isomer	*N3-cis-N7*	*N7-cis-N7*	*N7-trans-N7*	*N7-trans-py*
e_σ	4950[a]	5900[b]	5700[b]	4100[b]
e_π	400[a]	1850[b]	1650[b]	550[b]
e_σ(CN)	e_π(CN)	e_σ(N_{py})	e_π(N_{py})	e_σ(N_{amid})	e_π(N_{amid})
9300[b]	−1800[b]	7900[c]	−500[c]	8000[d]	2000[d]

[a]The $1/R^6$ dependence of the AOM parameters on the Cu–N bond lengths (see text) involves an adjustment to 2.052 Å for the *N3-cis-N7* and 2.168 Å for the other isomers; the normalized values are taken from ref 6. [b]AOM parameters from ref 39 normalized for a Fe^{III}–C distance of R = 1.904 Å. [c]AOM parameters from ref 37 normalized for an Fe^{III}–N distance of 1.968 Å. [d]AOM parameters obtained from a best fit to the g-tensors and energies of the d-d transitions of the Fe^{III} complex unit in *N7-trans-N7* (R(Fe^{III}–N_{amide}) = 1.900 Å.

Fe^{III} Sites. The analysis of the magnetic exchange in ferromagnetically coupled Cu^{II} (S = 1/2)–*low-spin* Fe^{III} (S = 1/2) dinuclear units in Cu-NC-Fe$(CN)_5$ model systems revealed a large anisotropy of the S = 1 spin ground state, due to unquenched orbital momentum of the Fe^{III} site ($^2T_2$ ground state).[34] This anisotropy arises from first order spin–orbit coupling which transmits the orbital momenta to the spin ground state, implying an orbital dependent exchange mechanism. It has been shown, that already tiny distortions due to the $^2T_2$ Fe^{III} ground state Jahn–Teller coupling can lift the orbital degeneracy and reduce the magnetic anisotropy. Symmetry reduction because of three different donors in the Fe^{III} coordination sphere of $[Fe(CN)_3(bpca)]^-$ was expected to lead to an even larger reduction of the magnetic anisotropy. This is supported by a comparison of the Fe^{III} g-tensor of the present *N7-trans-N7* isomer (g = 1.42, 2.29, 2.50) and that of the almost regular (axial) $[Fe(CN)_6]^{3-}$ species (g = 0.915, 2.100, 2.350).[40] From the AOM parameters for the Fe-CN and Fe–N_{py} bonds of Table 6 one infers that CN and N_{py} are strong σ-donors with Fe^{III}, and π-back bonding emerges from the negative e_π-values (large for Fe-CN [e_π = −1800 cm^{-1}] and modest for Fe–N_{py}, e_π = −500 cm^{-1}, see Figure 6 and Table 6).

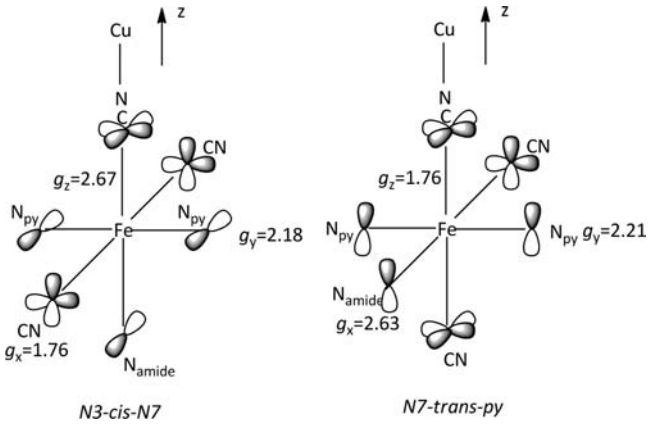

Figure 6. Fe^{III} π-bonding interactions and their correlation with the main values of the g tensor for the two different bridging arrangements in isomer *N3-cis-N7* and *N7-trans-py*.

With these parameter and the usual $1/R^6$ dependence, a reasonable fit of the e_σ and e_π values for the Fe–N_{amide} bond to the g-tensor values from the simulation of the EPR spectrum (Figure 3, Table 3) and the observed d-d transitions of the Fe^{III} site of the *N7-trans-N7* isomer (Table 2 and Supporting Information) are obtained. The resulting parameters (e_σ = 8,000 cm^{-1}, e_π = 2,000 cm^{-1}) endorse N_{amide} as a strong σ- and π-donor ligand. This is in agreement with the expectation and has been observed in earlier spectroscopic studies.[41] With the set of t_{2g} orbitals involved in π-interactions with the ligands the interplay between π-acceptor (Fe-CN, Fe–N_{py}) and π-donor (Fe–N_{amide}) leads to a t_{2g} orbital splitting pattern which can be easily deduced using the set of bonding parameters (Table 6) and AOM expressions (eq 5). For these expressions, the geometry of the FeC_3N_3 chromophore has been approximated as ortho-axial and π interactions between Fe- and in-plane orbitals of bpca have been neglected.

dx.doi.org/10.1021/ic301122h | *Inorg. Chem.* 2012, 51, 9357–9368

N3-cis-N7 [*N7-trans-py*]:

$$E(d_{yz})[E(d_{xy})] = e_\pi(CN) = -1800\ cm^{-1}$$

$$E(d_{xz})[E(d_{xz})] = 3e_\pi(CN) + e_\pi(N_{amide}) = 3\cdot(-1800) + 2000 = -3400\ cm^{-1}$$

$$E(d_{xy})[E(d_{yz})] = 2e_\pi(N_{py}) + 2e_\pi(CN) = 2\cdot(-500) + 2\cdot(-1800) = -4600\ cm^{-1} \quad (5)$$

With five electrons in the t_{2g} orbitals and neglecting orthorhombicity ^2E and $^2B_2$ type Fe^{III} ground states emerge (D_{4h} symmetry) for *N3-cis-N7* and *N7-trans-py*, respectively (Supporting Information). The orthorhombic ligand field and spin−orbit coupling lead to a strongly orthorhombic *g*-tensor at the Fe^{III} site, with an easy axis, as defined by the largest value of g = 2.6, parallel to NC-Fe-N_{amide} in both complexes. This is calculated to be parallel to the Fe-CN-Cu bond in the case of *N3-cis-N7* and perpendicular to this axis in the case of *N7-trans-py*. This has a crucial effect on the magnetic anisotropy of the entire Fe···Cu site.

Magnetic Anisotropy. A key observation is the change of the Fe^{III} ground state from $^2B(d_{xy}^2d_{xz}^2d_{yz}^1)$ in *N3-cis-N7* to $^2A(d_{xy}^1,d_{xz}^2,d_{yz}^2)$ in *N7-trans-py* (see Figure 8). In the pseudotetragonal D_{4h} symmetry the $^2T_{2g}$ octahedral ground state of Fe^{III} splits into $^2B_2$ and ^2E sublevels, and the latter has a first order angular momentum of ±1. With spin−orbit coupling and the low symmetry, these three sublevels are mixed and additionally split to result in three Kramers doublets (see Figure 7). Orbital-dependent exchange coupling between the

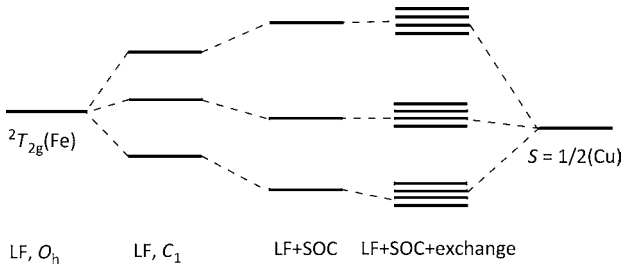

Figure 7. Correlation diagram illustrating the exchange coupling between the electronic ground states of Fe(III) and Cu(II) under the combined action of ligand field and spin−orbit coupling at the Fe(III) site and orbital dependent Fe−Cu anisotropic exchange.

Fe^{III} Kramers doublets and Cu^{II} leads to a total of 12 exchange-split multiplets, and these are illustrated in Figure 7. The combination of low symmetry and spin−orbit coupling results in four lowest nondegenerate electronic states, spanning an energy range of about 8 cm^{-1}, that is, of the same order of magnitude as reported on the basis of a DFT analysis of the magnetic anisotropy in a linear Cu-NC-Fe model complex.[34] Because of the lack of degeneracy in the two isomers discussed here, both are characterized by a nonmagnetic ground state which becomes magnetized in an applied magnetic field. The large spacing between these levels explains the EPR silence of the two complexes. In spite of the similar energy pattern of the spin levels in the two complexes, their wave function compositions are quite different (see Figure 8). The two lowest spin levels of *N3-cis-N7*, the ground state $^2B(d_{xy}^2d_{xz}^2d_{yz}^1)$ and the lowest excited state $^2B(d_{xy}^2d_{xz}^1d_{yz}^2)$, both of ^2E symmetry in D_{4h} are dominated by almost equal amounts of $|1,+1\rangle$ and $|1,-1\rangle$ functions. Therefore, a magnetic field along the *z*-axis induces magnetic moments along the Cu-NC-Fe (z) bond direction by mixing (polarization of the two nonmagnetic states). Mixing between the spin ground state and the $|1,0\rangle$ second excited state (^2A, $d_{xy}^1d_{xz}^2d_{yz}^2$) takes place with a magnetic field along the *x*-direction. However, because of the larger energy difference, the induced magnetic moment is much smaller (Figure 8). The situation drastically changes in *N7-trans-py*, where the ground state, $d_{xy}^2d_{xz}^2d_{yz}^1$ $|1,\pm1\rangle$ in *N3-cis-N7* changes to (^2A, $d_{xy}^1d_{xz}^2d_{yz}^2$). Here, mixing of the ground state (dominated by equal amounts of $|1,1\rangle$ and $|1,-1\rangle$) and the lowest excited state $|1,0\rangle$ via H_x dominates over mixing via H_z. The result is an easy axis magnetization in *N3-py-N7* in contrast to an easy plane magnetization in *N7-trans-py*. It follows that the change from easy axis to easy plane magnetizations (*N3-cis-N7* vs *N7-trans-py* isomers, respectively) is a direct consequence of orbital ordering, governed by the bridging topology at the Fe^{III} site.

Another striking difference between the two complexes emerges from the large antisymmetric exchange term which mixes a considerable amount of $|0,0\rangle$ singlet state character into the triplet state components $|1,\pm1\rangle$ of the *N7-trans-py* isomer, and this is not the case in the *N3-cis-N7* geometry. The origin of this difference is 2-fold: First, the Cu-NC-Fe bridge in both geometries is not linear (larger bending in *N7-trans-py*, see Table 1), and this leads to a larger antisymmetric exchange A_y. Second, there is a reorientation of the easy axis of the *g*-tensor from a direction approximately parallel to Cu-NC-Fe in the geometry *N3-cis-N7* to approximately perpendicular in the *N7-trans-py* isomer. This leads to a *g*-tensor asymmetry and results in a larger A_y value (see expressions in refs 42−44). Finally, antisymmetric exchange, leading to mixing of states of different spin multiplicity (see eq 4), is responsible for spin-canting effects, consisting in a weak antiferromagnetism (in *N3-cis-N7*, $D < 0$) or weak ferromagnetism (in *N7-trans-py*, $D > 0$, Figure 9). This may be quantified by the canting angle θ, calculated from D and A_y.[42] A small angle of $\theta = 3°$ for *N3-cis-N7* compared to a much larger for *N7-trans-py* correlates with a switch from an easy axis to an easy plane magnetic behavior.

CONCLUSION

The combination of the tris-cyanide-bpca-iron(III) with the cyanide-bispidine-copper(II) chromophores to cyanide-bridged heterodinuclear complexes allowed to thoroughly study the influence on the electronic properties of the distance and relative orientation involving the two S = 1/2 spin centers and the cyanide bridge. Of specific importance was the possibility to vary the local copper(II) geometry in terms of the bond strength and distance to the cyanide bridge. With the tetradentate bispidine ligand L^1, bonding to a monodentate coligand to complete a square pyramidal coordination sphere was known to occur perpendicular to the Jahn−Teller-elongated tertiary amine N7, in-plane with the tertiary amine N3 and the two pyridine groups.[21,45] A similar geometry in terms of the cyanide bridge is possible with the pentadentate bispidine ligand L^2, with the less common Jahn−Teller elongation along the two pyridine groups and the cyanide in-plane with the two tertiary amines N3 and N7, and the third pyridine donor, substituted to N7.[12,13] However, in this case

dx.doi.org/10.1021/ic301122h | *Inorg. Chem.* 2012, 51, 9357−9368

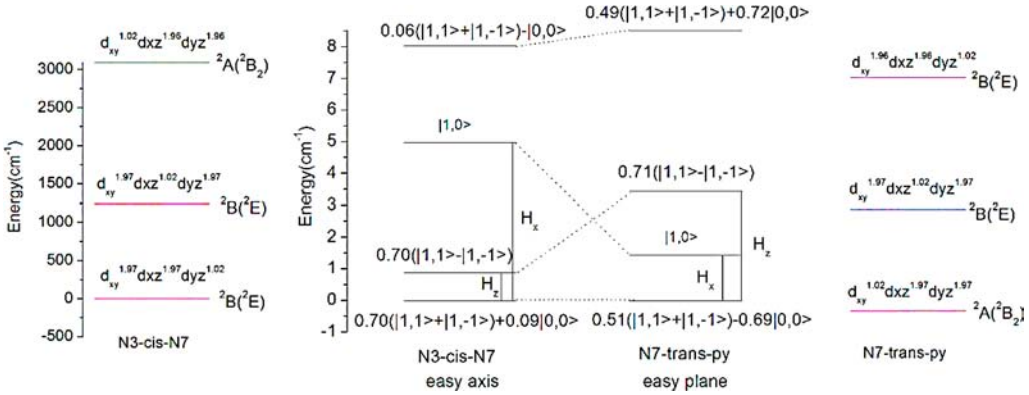

Figure 8. Spin-energy level diagram and wave function composition for *N3-cis-N7* and *N7-trans-py* resulting from the spin-Hamiltonian of eq 4 (H = 0) and anisotropic parameters from a fit to isothermal magnetization data (Table 4). The coupling of the spin-state of the electronic ground state with close-lying excited states in dependence of the direction of the applied magnetic field is shown. Plotted are the orbital configurations from which the sublevels of $[Fe(bpca)(CN)_3]^-$ ($^2T_2$ ground state) in *N3-cis-N7* and *N7-trans-py* emerge.

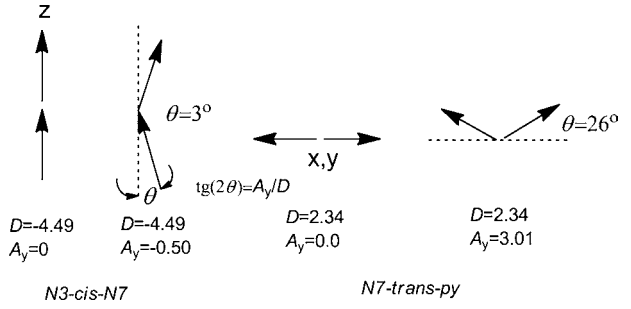

Figure 9. Spin-canting due to the simultaneous presence of axial anisotropy (D) and antisymmetric exchange (A_y) in the two isomers *N3-cis-N7* and *N7-trans-py*. Values of the canting angle θ, calculated classically, are only for visualization and should be viewed with caution.

the three possible "Jahn-Teller isomers" are close to degenerate and a selective stabilization of the more interesting, strongly coupled system is difficult. The two species with short Cu-NC distances (*N3-cis-N7* and *N7-trans-py* isomers) have very different electronic and magnetic properties, with small negative and positive axial zero-field splitting parameters D, respectively, a considerable orthorhombic anisotry (E) in both cases and, remarkably, a strongly antisymmetric exchange parameter A_y in the *N7-trans-py* isomer, related to the small but significant off-linearity of the Cu-NC-Fe bridge and the misfit between the direction of the largest component of the g-tensor and the Cu-NC-Fe axis.

EXPERIMENTAL SECTION

Measurements. *Powder UV−vis-NIR spectra* were recorded in Al_2O_3 with a V-570 UV−vis−NIR spectrophotometer (Jasco). *IR-spectra* were obtained from KBr pellets with a Spectrum 100 FT-IR-spectrometer (Perkin-Elmer). *ICP-emission-spectroscopy* was carried out on a Varian VISTA-MPX CCD Simultaneous ICP-OES device. For these measurements the complexes were destroyed with concentrated hydrochloric acid and then dissolved in an aqueous solution. *Magnetic measurements* were carried out on a MPMS-XL 5T (Quantum Design) SQUID magnetometer. Samples were powdered and pressed in PTFE tape to avoid field-induced orientation. The data were corrected for diamagnetism of the sample holder, and Pascal's constants were used for diamagnetic corrections of the sample.[46] For the simulation of the iso-field lines from the reduced magnetization data, the program julX was used.[47] *X-band EPR spectra* (9.5 GHz) were recorded on a Bruker Biospin ELEXSYS E-500 spectrometer with a cylindric resonator in TE_{101} modus. The system was equipped with an Oxford Instruments ESR 900 continuous liquid helium flow cryostat with a ITC 4 temperature controller. The spectra were simulated with MoSophe.[31] *Elemental analyses* were obtained from the microanalytical laboratory of the Chemical Institutes of the University of Heidelberg.

X-ray Crystal Structure Determinations. Crystal data and details of the structure determinations are given as Supporting Information. Intensity data were collected at low temperature with a STOE IPDS1 image plate system (Mo−K_α radiation, graphite monochromator, λ = 0.71073 Å). Absorption corrections of the data from the IPDS were done numerically, except for $[\{Fe(bpca)(CN)_3\}\{Cu(L^1\cdot H_2O)\}]BF_4$, since a correction did not improve the structural data. The structures were solved by the heavy atom method and refined by full-matrix least-squares methods based on F^2 against all unique reflections.[48,49] All non-hydrogen atoms were given anisotropic displacement parameters.

DFT Calculations. The data presented are based on single-point calculations, using coordinates from the experimental structures. To obtain structurally comparable systems, the X-ray data were modified such that in all structures there is a ketone at C9. Calculations were done with Gaussian09,[50] with the B3LYP functional,[51] and the TZVP basis set.[52] The isotropic exchange constants J were obtained with the usual broken-symmetry approach,[53] with a computational setup tested and validated for the type of complexes used in the present communication.[35]

Syntheses. *General Information, Ligands, and Precursors.* Chemicals were used as supplied. Technical grade solvents were distilled prior to use. The ligands L^1 and L^2 as well as their Cu^{II} complexes were prepared as described previously.[54−56] *$[Fe^{II}(bpca)_2]$*, *$[Fe^{III}(bpca)(Cl)_2(OH_2)]$*, as well as *$[N(^tbu)_4][Fe^{III}(bpca)(CN)_3]$* were prepared according to known procedures.[27,57] The purity of the precursors was checked by elemental analyses, high resolution mass spectroscopy, and infrared spectroscopy. *Bis(2-pyridylcarbonyl)amine* was synthesized similar to a known procedure:[58] 1,3,5-tris(2-pyridyl)triazin and $CuSO_4$ were refluxed in water for 30 min. For a quantitative precipitation the blue suspension was stored at 4 °C overnight. After filtration the solid was suspended in a mixture of water/chloroform, and Na_2H_2EDTA was added to the suspension. To the mixture, 1 equiv of NaOH [with respect to 1,3,5-tris(2-pyridyl)triazine] was added and stirred for 45 min. The organic phase was separated, and the aqueous solution was extracted with chloroform several times. The pale green organic solution was dried in Na_2SO_4 and filtrated via silica gel. The solvent was removed under reduced pressure and dried under vacuum. The purity of the white product (yield: 56%) was checked via ^1H NMR spectroscopy, elemental analyses, and high resolution mass spectroscopy.

$[\{Fe(bpca)(CN)_3\}\{Cu(L^1)\}]PF_6\cdot 2H_2O$ (N3-cis-N7-isomer). To a solution of $[Cu(L^1)(NCMe)(OH_2)](PF_6)_2$ (170 mg, 0.2 mmol) in a 1/1 mixture of $MeCN/CH_2Cl_2$ (8 mL), $[N(^tbu)_4][Fe^{III}(bpca)(CN)_3]$ (120 mg; 0.2 mmol) in CH_2Cl_2 (8 mL) was added dropwise at room temperature. After a short period a green solid formed rapidly, which

dx.doi.org/10.1021/ic301122h | Inorg. Chem. 2012, 51, 9357−9368

was filtrated and washed with a small amount of MeOH. The green product was dried under vacuum. Yield 107 mg (51%). Anal. (%) Calcd for $[\{Fe(bpca)(CN)_3\}\{Cu(L^1)\}]PF_6\cdot 2H_2O$: C, 43.75; H, 3.67; N, 13.43. Found: C, 43.52; H, 3.85; N, 13.42. IR ν(C≡N): 2120; 2126; 2173 cm^{-1}. ICP-OES (Fe:Cu): 1.05: 1. UV−vis (powder, Al_2O_3), [cm^{-1}]; d-d (Cu^{II}): 9400 (sh); 16,550. Single crystals for X-ray crystallography were obtained for *$[\{Fe(bpca)(CN)_3\}\{Cu(L^1\cdot H_2O)\}]BF_4$*.[11,14−16,19,56] To a solution of $[N(^tbu)_4][Fe^{III}(bpca)(CN)_3]$ (61 mg; 0.1 mmol) in MeOH (60 mL), $[Cu(L^1)(OH_2)_2](BF_4)_2\cdot H_2O$ (73 mg; 0.1 mmol) was added in small portions. The reaction mixture was briefly heated to boiling temperature and left for crystallization by slow evaporation of the solvent.

$[\{Fe(bpca)(CN)_3\}\{Cu(L^2)\}][Fe(bpca)(CN)_3]\cdot 5H_2O$ (N7-cis-N7-isomer). To a solution of $[Cu(L^2)(OH_2)](PF_6)_2\cdot H_2O$ (90.5 mg, 0.1 mmol), in MeCN (10 mL), $[N(^tbu)_4][Fe(bpca)(CN)_3]$ (60 mg, 0.1 mmol), in CH_2Cl_2 (8 mL), was added dropwise at room temperature and stirred for a short period of time. Single crystals were obtained after a few days by slow evaporation of the solvent at room temperature. The green product was vacuum-dried. Yield 58 mg (83%). Anal. (%) Calcd for $[\{Fe(bpca)(CN)_3\}\{Cu(L^2)\}][Fe(bpca)(CN)_3]\cdot 5H_2O$: C, 50.14; H, 3.99; N, 17.14. Found: C, 50.03; H, 4.02; N, 17.11. IR ν(C≡N): 2124; 2133 cm^{-1}. UV−vis (powder, Al_2O_3) [cm^{-1}]; d-d (Cu^{II}): 8900; 15,200.

$[\{Fe(bpca)(CN)_3\}\{Cu(L^2\cdot MeOH)\}]PF_6\cdot MeOH\cdot H_2O$ (N7-trans-N7-isomer). To a solution of $[Cu(L^2)(OH_2)](PF_6)_2\cdot H_2O$ (181 mg, 0.2 mmol) in MeOH (50 mL) $[N(^tbu)_4][Fe(bpca)(CN)_3]$ (60 mg, 0.1 mmol), in MeOH (10 mL), was added dropwise at room temperature. The green reaction mixture was concentrated to half, and diethyl ether was slowly diffused into the solution at room temperature. Single crystals were obtained after a few days. The green product was vacuum-dried. Yield 55 mg (47%). Anal. (%) Calcd for $[\{Fe(bpca)(CN)_3\}\{Cu(L^2\cdot MeOH)\}]PF_6\cdot MeOH\cdot H_2O$: C, 46.34; H, 4.06; N, 13.21. Found: C, 46.43; H, 4.08; N, 13.08. IR ν(C≡N): 2127; 2135 cm^{-1}. UV−vis (powder Al_2O_3) [cm^{-1}]; d-d (Cu^{II}): 8900; 15,200.

$[\{Fe(bpca)(CN)_3\}\{Cu(L^2)\}]PF_6\cdot 2H_2O$ (N7-trans-py-isomer). To a solution of $[Cu(L^2)(OH_2)](PF_6)_2\cdot H_2O$ (181 mg, 0.2 mmol), in MeCN (5 mL), $[N(^tbu)_4][Fe(bpca)(CN)_3]$ (60 mg, 0.1 mmol), in CH_2Cl_2 (10 mL), was added dropwise at room temperature. The green reaction mixture was concentrated to half, and diethyl ether was slowly diffused at 4 °C into the solution. Single crystals could be obtained after a few days. The green product was washed with a small amount of MeOH and dried under vacuum. Yield 78 mg (69%). Anal. (%) Calcd for $[\{Fe(bpca)(CN)_3\}\{Cu(L^2)\}]PF_6\cdot 2H_2O$: C, 46.10; H, 3.69; N, 13.75. Found: C, 46.27; H, 3.58; N, 13.80. IR ν(C≡N): 2117; 2129 2144 cm^{-1}. UV−vis (powder, Al_2O_3) [cm^{-1}]; d-d (Cu^{II}): 8400; 14,400.

■ ASSOCIATED CONTENT

Ⓢ Supporting Information

Details of the DFT and ligand field calculations, IR and electronic spectra. This also includes the crystallographic data table and cif files. This material is available free of charge via the Internet at http://pubs.acs.org. CCDC 884083−884086 contains the supplementary crystallographic data for this paper. These data can be obtained free of charge from The Cambridge Crystallographic Data Centre via www.ccdc.cam.ac.uk/data_request/cif.

■ AUTHOR INFORMATION

Corresponding Author

*Fax: +49-6226-546617. E-mail: peter.comba@aci.uni-heidelberg.de (P.C.), Mihail.Atanasov@cec.mpg.de (S.H.).

Notes

The authors declare no competing financial interest.

■ ACKNOWLEDGMENTS

Financial support by the German Science Foundation (DFG) is gratefully acknowledged. We thank Dr. Thomas Zessin and Prof. Hubert Wadepohl for helpful discussions related to crystallography, and Philipp Butzug for crystallographic measurements.

■ REFERENCES

(1) Sessoli, R.; Gatteschi, D. *Angew. Chem., Int. Ed.* **2003**, *42*, 243.
(2) Solomon, E. I.; Ginsbach, J. W.; Heppner, D. E.; Kieber-Emmons, M. T.; Kjaegaard, C. H.; Smeets, P. J.; Tian, L.; Woertink, J. S. *Faraday Discuss.* **2011**, *148*, 11.
(3) Beltran, L. M. C.; Long, J. R. *Acc. Chem. Res.* **2005**, *38*, 325.
(4) Atanasov, M.; Comba, P.; Hausberg, S.; Martin, B. *Coord. Chem. Rev.* **2009**, *253*, 2306.
(5) Atanasov, M.; Comba, P.; Daul, C. A. *J. Phys. Chem. A* **2006**, *110*, 13332.
(6) Atanasov, M.; Comba, P.; Hanson, G. R.; Hausberg, S.; Helmle, S.; Wadepohl, H. *Inorg. Chem.* **2011**, *50*, 6890.
(7) Bleaney, B.; Bowers, K. D. *Proc. R. Soc. London, Ser. A* **1952**, *214*, 451.
(8) Ozarowski, A. *Inorg. Chem.* **2008**, *47*, 9760.
(9) Glaser, T. *Chem. Commun.* **2011**, *47*, 116.
(10) Neese, F.; Pantazis, D. A. *Faraday Discuss.* **2011**, *148*, 229.
(11) Comba, P.; Kerscher, M.; Schiek, W. *Prog. Inorg. Chem.* **2007**, *55*, 613.
(12) Comba, P.; Hauser, A.; Kerscher, M.; Pritzkow, H. *Angew. Chem., Int. Ed.* **2003**, *42*, 4536.
(13) Bentz, A.; Comba, P.; Deeth, R. J.; Kerscher, M.; Pritzkow, H.; Seibold, B.; Wadepohl, H. *Inorg. Chem.* **2008**, *47*, 9518.
(14) Comba, P.; Nuber, B.; Ramlow, A. *J. Chem. Soc., Dalton Trans.* **1997**, 347.
(15) Börzel, H.; Comba, P.; Hagen, K. S.; Merz, M.; Lampeka, Y. D.; Lienke, A.; Linti, G.; Pritzkow, H.; Tsymbal, L. V. *Inorg. Chim. Acta* **2002**, *337*, 407.
(16) Comba, P.; Kerscher, M.; Merz, M.; Müller, V.; Pritzkow, H.; Remenyi, R.; Schiek, W.; Xiong, Y. *Chem.—Eur. J.* **2002**, *8*, 5750.
(17) Gleiter, R.; Kobayashi, M.; Kuthan, J. *Tetrahedron* **1976**, *32*, 2775.
(18) Atanasov, M.; Busche, C.; Comba, P.; El Hallak, F.; Martin, B.; Rajaraman, G.; van Slageren, J.; Wadepohl, H. *Inorg. Chem.* **2008**, *47*, 8112.
(19) In metal complexes, the keto group at C9 is often hydrolyzed, and this reaction is not easy to control.[11,14−16,56] In the present work, the X-ray and the spectroscopic and magnetic data are from two different samples. The tetrafluoroborate salt (X-ray) indicates that the keton is hydrolyzed, and this probably (but not unambiguously) is also the case for the sample used for spectroscopy and magnetism (see elemental analysis).
(20) In our hands and with the procedures described in the Experimental Section, the isolation of the two isomers N7-cis-N7 and N7-trans-N7 was fully reproducible; however, isolation of the isomer N7-trans-py only occurred once.
(21) Comba, P.; Kerscher, M.; Roodt, A. *Eur. J. Inorg. Chem.* **2004**, *23*, 4640.
(22) Comba, P.; Lopez de Laorden, C.; Pritzkow, H. *Helv. Chim. Acta* **2005**, *88*, 647.
(23) Note that because we did not use geometry-optimized but the crystal structural data, solvation has not been considered and because of a general accuracy of the computational setup used of approximately 10−15 kJ/mol,[24] these relative energies have to be considered with some care.
(24) Siegbahn, P. E. M.; Borowski, T. *Acc. Chem. Res.* **2006**, *39*, 729.
(25) The $[Fe(bpca)(CN)_3]$-building block and corresponding oligonuclear complexes have been described before, see, e.g., refs 26,27 and some of our conclusions with respect of the electronic structures are supported by these earlier studies.

(26) Lescouëzec, R.; Vaissermann, J.; Toma, L. M.; Carrasco, R.; Lloret, F.; Julve, M. *Inorg. Chem.* **2004**, *43*, 2234.
(27) Wen, H.-R.; Wang, C.-F.; Zuo, J.-L.; Song, Y.; Zeng, X.-R.; You, X.-Z. *Inorg. Chem.* **2006**, *45*, 582.
(28) Ozarowski, A.; Reinen, D. *Inorg. Chem.* **1986**, *25*, 1704.
(29) Ni, Z.-H.; Kou, H.-Z.; Zhang, L.-F.; Ni, W.-W.; Jiang, Y.-B.; Cui, A.-L.; Ribas, J.; Sato, O. *Inorg. Chem.* **2005**, *44*, 9631.
(30) A low-energy charge transfer transition might also occur in this area.
(31) Hanson, G. R.; Noble, C. J.; Benson, S. *High Resolution EPR: Applications to Metalloenzymes and Metals in Medicine*; Hanson, G. R., Berliner, L. J., Eds.; Springer: New York, **2009**; Vol. *28*, p 105.
(32) Toma, L. M.; Delgado, F. S.; Ruiz-Pérez, C.; Carrasco, R.; Cano, J.; Lloret, F.; Julve, M. *Dalton Trans.* **2004**, 2836.
(33) Neither of the four complexes are strictly highly symmetrical. However, in a good approximation a symmetry plane including the three CN groups and N_{amide} can be defined which in each case leads to an antisymmetric vector nearly parallel to the N_{py}-Fe-N_{py} bond direction.
(34) Atanasov, M.; Comba, P.; Daul, C. A. *Inorg. Chem.* **2008**, *47*, 2449.
(35) Comba, P.; Hausberg, S.; Martin, B. *J. Phys. Chem. A* **2009**, *113*, 6751.
(36) Comba, P.; Hambley, T. W.; Hitchman, M. A.; Stratemeier, H. *Inorg. Chem.* **1995**, *34*, 3903.
(37) Comba, P. *Coord. Chem. Rev.* **1999**, *182*, 343.
(38) Atanasov, M.; Comba, P.; Martin, B.; Müller, V.; Rajaraman, G.; Rohwer, H.; Wunderlich, S. *J. Comput. Chem.* **2006**, *27*, 1263.
(39) Atanasov, M.; Comba, P.; Daul, C. A.; Hauser, A. *J. Phys. Chem., A* **2007**, *111*, 9145.
(40) Baker, J. M.; Bleaney, B.; Bowers, K. D. *Proc. Phys. Soc., Sect. B* **1956**, *69*, 1205.
(41) Schmidtke, H.-H.; Schönherr, T.; Kuchen, W.; Fuchs, M. *Chem. Phys. Lett.* **1986**, *124*, 159.
(42) Moriya, T. In *Magnetism*; Rado, G. T.; Suhl, H., Eds.; Academic Press: New York, 1963; Vol. *1*, p 85.
(43) Kanamori, J. In *Magnetism*; Rado, G. T., Suhl, H., Eds.; Academic Press: New York, 1963; Vol. *1*, p 127.
(44) Bencini, A.; Gatteschi, D. *Electron Paramagnetic Resonance of Exchange coupled systems*; Springer: Berlin, Germany, 1990; p 27.
(45) Comba, P.; Lienke, A. *Inorg. Chem.* **2001**, *40*, 5206.
(46) Pascal, P.; Pacault, A.; Hoarau, J. *C. R. Acad. Sci.* **1951**, *233*, 1078.
(47) Bill, E. *julX*; Max-Plank Institute of Bioinorganic Chemistry, MPI für Bioanorganische Chemie: Mülheim, Germany; http://ewww.mpi-muelheim.mpg.de/bac/logins/bill/juIX_en.php.
(48) Sheldrick, G. M. *SHELXL-97*; University of Göttingen: Göttingen, Germany, 1997.
(49) Sheldrick, G. M. *Acta Crystallogr.* **2008**, *A64*, 112.
(50) Frisch, M. J.; Trucks, G. W.; Schlegel, H. B.; Scuseria, G. E.; Robb, M. A.; Cheeseman, J. R.; Scalmani, G.; Barone, V.; Mennucci, B.; Petersson, G. A.; Nakatsuji, H.; Caricato, M.; Li, X.; Hratchian, H. P.; Izmaylov, A. F.; Bloino, J.; Zheng, G.; Sonnenberg, J. L.; Hada, M.; Ehara, M.; Toyota, K.; Fukuda, R.; Hasegawa, J.; Ishida, M.; Nakajima, T.; Honda, Y.; Kitao, O.; Nakai, H.; Vreven, T.; Montgomery Jr., J. A.; Peralta, J. E.; Ogliaro, F.; Bearpark, M.; Heyd, J. J.; Brothers, E.; Kudin, K. N.; Staroverov, V. N.; Kobayashi, R.; Normand, J.; Raghavachari, K.; Rendell, A.; Burant, J. C.; Iyengar, S.; Tomasi, J.; Cossi, M.; Rega, N.; Millam, N. J.; Klene, M.; Knox, J. E.; Cross, J. B.; Bakken, V.; Adamo, C.; Jaramillo, J.; Gomperts, R.; Stratmann, R. E.; Yazyev, O.; Austin, A. J.; Cammi, R.; Pomelli, C.; Ochterski, J. W.; Martin, R. L.; Morokuma, K.; Zakrzewski, V. G.; Voth, G. A.; Salvador, P.; Dannenberg, J. J.; Dapprich, S.; Daniels, A. D.; Farkas, O.; Foresman, J. B.; Ortiz, J. V.; Cioslowski, J.; Fox, D. J. *Gaussian 09*, Revision A.02; Gaussian, Inc.: Wallingford, CT, 2009.
(51) Becke, A. D. *J. Chem. Phys.* **1993**, *98*, 5648.
(52) Schäfer, A.; Huber, C.; Ahlrichs, R. *J. Chem. Phys.* **1994**, *100*, 5829.
(53) Noodleman, L. *J. Chem. Phys.* **1981**, *74*, 5737.
(54) Börzel, H.; Comba, P.; Katsichtis, C.; Kiefer, W.; Lienke, A.; Nagel, V.; Pritzkow, H. *Chem.—Eur. J.* **1999**, *5*, 1716.
(55) Börzel, H.; Comba, P.; Hagen, K. S.; Kerscher, M.; Pritzkow, H.; Schatz, M.; Schindler, S.; Walter, O. *Inorg. Chem.* **2002**, *41*, 5440.
(56) Comba, P.; Merz, M.; Pritzkow, H. *Eur. J. Inorg. Chem.* **2003**, 1711.
(57) Wocadlo, S.; Massa, W.; Folgado, J. V. *Inorg. Chim. Acta* **1993**, *207*, 199.
(58) Kamiyama, A.; Noguchi, T.; Kajiwara, T.; Ito, T. *Inorg. Chem.* **2002**, *41*, 507.
(59) Wang, C.-F.; Zuo, J.-L.; Bartlett, B. M.; Song, Y.; Long, J. R.; You, X.-Z. *J. Am. Chem .Soc.* **2006**, *128*, 7162.
(60) Gu, Z.-G.; Liu, W.; Yang, Q.-F.; Zhou, X.-H.; Zuo, J.-L.; You, X.-Z. *Inorg. Chem.* **2007**, *46*, 3236.
(61) Rodriguez-Fortea, A.; Alemany, P.; Alvarez, S.; Ruiz, E.; Scuiller, A.; Decroix, C.; Marvaud, V.; Vaissermann, J.; Verdaguer, M.; Rosenman, I.; Julve, M. *Inorg. Chem.* **2001**, *40*, 5868.
(62) Oshio, H.; Yamamoto, M.; Ito, T. *Inorg. Chem.* **2002**, *41*, 5817.
(63) *POV-Ray*, 3.6 ed.; Persistence of Vision Raytracer Pty. Ltd.: Williamstown, Australia, 2005.